AIP | Review of Scientific Instruments

Multi-channel lock-in amplifier assisted femtosecond time-resolved fluorescence non-collinear optical parametric amplification spectroscopy with efficient rejection of superfluorescence background

Pengcheng Mao, Zhuan Wang, Wei Dang, and Yuxiang Weng

Citation: Review of Scientific Instruments **86**, 123113 (2015); doi: 10.1063/1.4938187
View online: http://dx.doi.org/10.1063/1.4938187
View Table of Contents: http://scitation.aip.org/content/aip/journal/rsi/86/12?ver=pdfcov
Published by the AIP Publishing

Articles you may be interested in

Prediction of pulse-to-pulse intensity fluctuation characteristics of high power ultrafast fiber amplifiers
Appl. Phys. Lett. **105**, 011111 (2014); 10.1063/1.4888298

Coherent photon interference elimination and spectral correction in femtosecond time-resolved fluorescence non-collinear optical parametric amplification spectroscopy
Rev. Sci. Instrum. **84**, 073105 (2013); 10.1063/1.4812344

Light amplification at 501 nm and large nanosecond optical gain in organic dye-doped polymeric waveguides
Appl. Phys. Lett. **88**, 161114 (2006); 10.1063/1.2197314

Femtosecond transient fluorescence spectrometer based on parametric amplification
Appl. Phys. Lett. **86**, 021909 (2005); 10.1063/1.1850591

Coherent interactions in femtosecond transient grating
J. Chem. Phys. **120**, 5269 (2004); 10.1063/1.1647534

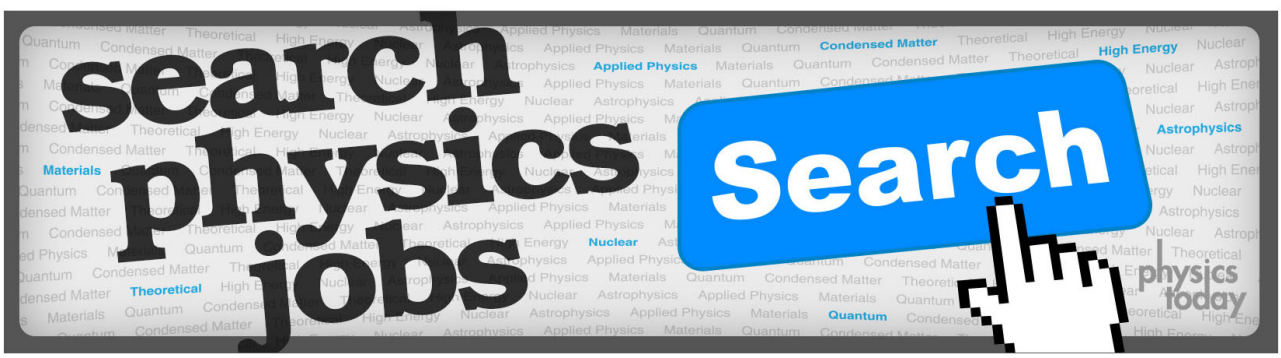

This article is copyrighted as indicated in the article. Reuse of AIP content is subject to the terms at: http://scitationnew.aip.org/termsconditions. Downloaded to IP: 159.226.35.239 On: Wed, 30 Dec 2015 07:54:51

Multi-channel lock-in amplifier assisted femtosecond time-resolved fluorescence non-collinear optical parametric amplification spectroscopy with efficient rejection of superfluorescence background

Pengcheng Mao, Zhuan Wang, Wei Dang, and Yuxiang Weng[a)]
Key Laboratory of Soft Matter Physics, Beijing National Laboratory for Condensed Matter Physics, Institute of Physics, Chinese Academy of Sciences, Beijing 100190, China

(Received 24 June 2015; accepted 7 December 2015; published online 29 December 2015)

Superfluorescence appears as an intense background in femtosecond time-resolved fluorescence noncollinear optical parametric amplification spectroscopy, which severely interferes the reliable acquisition of the time-resolved fluorescence spectra especially for an optically dilute sample. Superfluorescence originates from the optical amplification of the vacuum quantum noise, which would be inevitably concomitant with the amplified fluorescence photons during the optical parametric amplification process. Here, we report the development of a femtosecond time-resolved fluorescence non-collinear optical parametric amplification spectrometer assisted with a 32-channel lock-in amplifier for efficient rejection of the superfluorescence background. With this spectrometer, the superfluorescence background signal can be significantly reduced to 1/300–1/100 when the seeding fluorescence is modulated. An integrated 32-bundle optical fiber is used as a linear array light receiver connected to 32 photodiodes in one-to-one mode, and the photodiodes are further coupled to a home-built 32-channel synchronous digital lock-in amplifier. As an implementation, time-resolved fluorescence spectra for rhodamine 6G dye in ethanol solution at an optically dilute concentration of 10^{-5}M excited at 510 nm with an excitation intensity of 70 nJ/pulse have been successfully recorded, and the detection limit at a pump intensity of 60 μJ/pulse was determined as about 13 photons/pulse. Concentration dependent redshift starting at 30 ps after the excitation in time-resolved fluorescence spectra of this dye has also been observed, which can be attributed to the formation of the excimer at a higher concentration, while the blueshift in the earlier time within 10 ps is attributed to the solvation process. © *2015 AIP Publishing LLC.* [http://dx.doi.org/10.1063/1.4938187]

I. INTRODUCTION

Ultrafast time-resolved fluorescence spectroscopy is a useful method in the study of energy and electron transfer occurring in the photophysical and photochemical processes of the excited states.[1–9] Unlike the ultrafast time-resolved transient absorption spectra, it usually gives the straightforward information regarding the lowest fluorescence excited state. To acquire ultrafast time-resolved fluorescence spectra, a number of detection techniques such as Kerr gating, streak camera, up-conversion and fluorescence non-collinear optical parametric amplification spectroscopy (FNOPAS) with their unique advantages as well as limitations have been developed. Commercial streak camera is more popular for its simple optical alignment, broad spectral-, and large dynamical ranges. However, its temporal resolution is limited to 1 ps.[3,5] Kerr gating method, with the advantage of broad spectral acceptance, is limited by the requirement of high pulse energy for gating and residual transmittance of the Kerr shutter which reduces the temporal resolution.[6,7,10,11] In 2003, Gilch's group realized 100 fs time resolution in a near IR pumped broadband Kerr gating setup.[8] Up-conversion technique is superior for its temporal resolution as high as that of the laser pulse width, owing to the requirement of the phase matching condition, the angle of nonlinear crystal has to be optimized for different wavelengths to cover the broadband spectrum.[9,12–14] In 2009, Eom *et al.* provided 40 fs time resolution for the whole emission wavelength range in the investigation of polar solvation dynamics of Coumarin 153.[9] Recently, broadband spectrum as wide as 26 000 cm^{-1} was obtained by the combination of down- and up-conversions with a fixed geometry by Ernsting's group.[15,16] Compared with the traditional up-conversion system, their collected fluorescence cone is varied 5° to meet the needs of phase matching condition of different wavelengths with the collective optics and a prism. Fluorescence non-collinear optical parametric amplification spectroscopy is a newly developed technique for recording ultrafast time-resolved broadband fluorescence spectra.[17–21] The proof-in-principle experiment was demonstrated by Fita *et al.* in the visible range.[17] Soon after, our group extended the seeding fluorescence to the near IR region,[18] and the fluorescence decay kinetics together with the time-resolved spectra can be obtained by its conjugated part in the visible region. Later, we reported a gain factor of 10^5–10^6,[19] a detection limit of about 20 photons/pulse for noncoherent seeding light,[19,22] and a single photon/pulse for coherent seeding light[23] for a 120 fs pulsed laser, spectral correction method by using the inherent spectrum of the vacuum quantum noise which would be amplified as the superfluorescence concomitant with the amplified fluorescence,[20] and Cassegrain objective for fluorescence collection to remove the possible

a)Author to whom correspondence should be addressed. Electronic mail: yxweng@aphy.iphy.ac.cn

 © 2015 AIP Publishing LLC
This article is copyrighted as indicated in the article. Reuse of AIP content is subject to the terms at: http://scitationnew.aip.org/termsconditions. Downloaded to IP: 159.226.35.239 On: Wed, 30 Dec 2015 07:54:51

interference from the white light continuum generation.[21] It has been reported that the amplified signal of non-collinear optical parametric amplification (NOPA) could be tuned from 460 to 1150 nm in a signal branch, the corresponding tuning range for the idler beam would be 600 nm to 2800 nm.[24] And we have shown that the bandwidth of more than 100 nm (2500 cm^{-1}) with a relatively uniform gain curve (normalized value in the range of 0.8–1.0) could be achieved at a fixed phase-matched angle.[20] In principle, the detectable fluorescence spectral range can cover 460 to 2800 nm in combination with rotation of the beta barium borate (BBO) angle. We also successfully applied FNOPAS in a number of practical cases, such as detection of photogenerated carrier relaxation dynamics in CdS_xSe_{1-x},[25] ultrafast energy transfer in photosynthetic process for marine algae and for artificial photosynthetic systems,[26,27] and characterization of the lasing dynamics in organic waveguide with a length about 500 nm.[28] With our continuous efforts, FNOPAS could achieve a time resolution comparable to the width of the excitation laser pulse and can be used to acquire time-resolved fluorescence spectra with a good spectral fidelity.

However, the concomitant parametric superfluorescence in FNOPAS is an unavoidable background interference in the time-resolved amplified fluorescence spectra. Parametric superfluorescence is the amplified quantum noise due to zero-point fluctuations[29,30] in the absence of the signal or idler input at a condition of high gain of the nonlinear media.[31] It has been shown recently that the parametric fluorescence has the same amplification behavior as the purposely applied seeding beam at the signal wavelength. Both the parametric fluorescence and seeding light enter linearly into the output and the pump leads to exponential amplification. Zero-point fluctuations at both the signal and the idler wavelength range contribute to the parametric superfluorescence.[32] Therefore, the parametric fluorescence can hardly be removed physically from the amplified fluorescence, in principle, as well as in practice. Owing to its fluctuation by nature, it would bring a large fluctuation in the intensity of amplified seeded fluorescence, especially when the amplified fluorescence is much weaker than the parametric superfluorescence. In our previous work, when the amplified fluorescence is more intense than the parametric superfluorescence, multi-wavelength acquisition of the time-resolved fluorescence spectra can be realized with a polychromator assisted with an array detector or charge coupled device (CCD) matrix. The parametric fluorescence background was subtracted by data post-processing, i.e., subtracting the mixed spectra of amplified fluorescence and parametric fluorescence by an independently acquired background parametric fluorescence spectrum scaled by an appropriate factor. Apparently, when the superfluorescence is more intense than the amplified fluorescence, this method becomes invalid. This greatly limits the application of FNOPAS. In contrast, single wavelength detection of kinetics at this condition is still possible by the use of a conventional single-channel lock-in amplifier, for a lock-in amplifier which can detect AC signals even if when they are overwhelmed by much larger noise components. This is realized by selecting an appropriate reference modulation frequency on the signals.[33,34] With this method, the detection limit for the single wavelength detection has been determined as about 20 photons/pulse for noncoherent seeding light[19,22] and down to one photon/pulse for coherent seeding light.[23]

In principle, it is possible to construct the time-resolved fluorescence spectra by the acquisition of the single-wavelength amplified fluorescence decay kinetics using single-channel lock-in amplifier method at every selected wavelength; however, this would take a long time, and the problem of long-term stability of the laser system would definitely prevent the construction of reliable time-resolved fluorescence spectra. Consequently, an idealized apparatus for acquisition of time-resolved fluorescence spectra based on FNOPAS should combine the advantages of simultaneous detection of multi-wavelengths like array detector or CCD and rejection of the parametric fluorescence signals as the lock-in amplifier. Recently, Kobayashi's group used multi-channel lock-in detection in stimulated Raman microscope for spectral imaging to obtain spontaneous Raman scattering spectra with high temporal synchronization. The multi-channel lock-in detection improves imaging not only by increasing the speed being multiplied by the channel number but also by alleviating problems such as laser fluctuations and sample damage by simultaneously measuring the full Raman spectral range of interest.[34]

Towards this purpose, in this work, we proposed a new detection system for FNOPAS by using a 32-bundle optical fiber arranged in a linear array at the focal plane of the spectrometer, and the exit ends were connected to 32 photodiodes coupled to a 32-channel lock-in amplifier. With this apparatus, we realized nearly background-free femtosecond time-resolved broadband spectra detection, and the time-resolved fluorescence spectra for rhodamine 6G dye in ethanol solution at an optically dilute concentration as low as 10^{-5}M with an excitation intensity as low as 70 nJ/pulse at 510 nm have been successfully recorded. We have clearly illustrated that the dynamics for the solvation process is at the initial stage within 10 ps with a blueshift in the time-resolved fluorescence spectra, while the formation of the excimer at a higher concentration started at about 30 ps after the excitation with a significant redshift in fluorescence spectra.

II. EXPERIMENTAL SETUP

A. Optical setup

The optical setup is shown in Fig. 1. A Ti:Sapphire regenerative amplifier (Spitfire Ace, 3.5 W, Spectra Physics) with a repetition rate of 1 kHz provides p-polarized laser pulses of 35 fs in pulse-width at 800 nm. The output beam is split with a 50:50 beam splitter (BS1). The transmitted beam is used to excite the sample while the reflected beam is used as the pump beam for the fluorescence amplification in a BBO crystal. Half-wave plates WP1 and WP3 rotate the polarizations of the excitation and pump beams, respectively, by 90° to realize the phase matching condition of NOPA and FNOPAS. Both of BBO crystals for NOPA and FNOPAS are cut for type I phase matching. 1% of the transmitted beam is reflected by the second beam splitter (BS2) and is focused on a c-cut sapphire plate (S) to generate white

This article is copyrighted as indicated in the article. Reuse of AIP content is subject to the terms at: http://scitationnew.aip.org/termsconditions. Downloaded to IP: 159.226.35.239 On: Wed, 30 Dec 2015 07:54:51

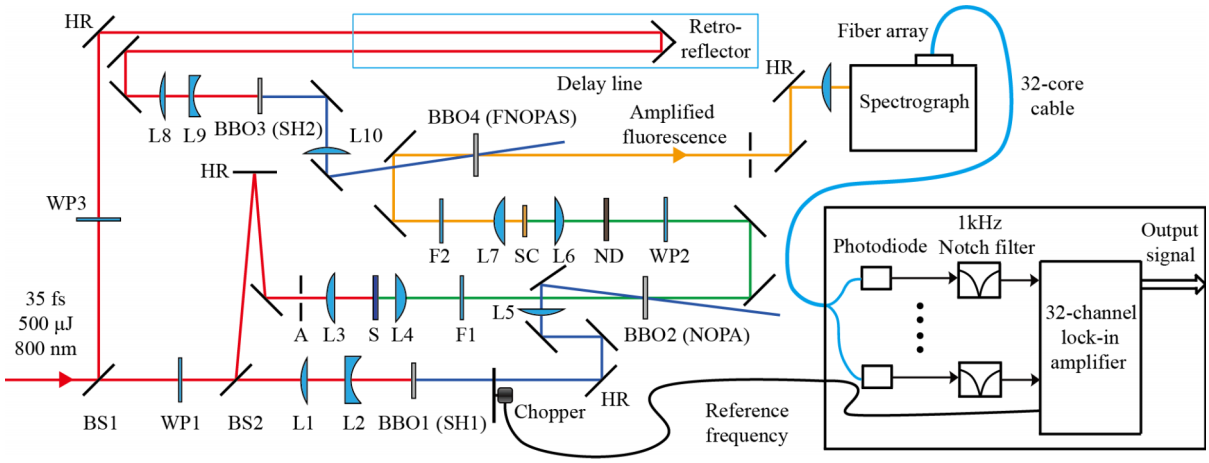

FIG. 1. Schematic diagram for the setup of multi-channel lock-in amplifier assisted femtosecond time-resolved fluorescence non-collinear optical parametric amplification spectroscopy. HR, high reflective mirror at specific wavelength; BS1, 50:50 beam splitter; BS2, 99:1 (T:R) beam splitter; WP1 and WP3, $\lambda/2$ wave plate at 800 nm; WP2, achromatic $\lambda/2$ wave plate (400–800 nm); L, lenses; A, continuously variable aperture; S, c-cut sapphire; SC, sample cell; ND, neutral density filter; F1, notch filter centered at 800 nm; F2, long pass filter for elimination of the excitation beam; BBO1 and BBO3, 1 mm thick BBO crystal cut at $\theta = 29.2°$ for second harmonic generation (SH1 and SH2); BBO2 and BBO4, 1 mm thick BBO crystal cut at $\theta = 31.7°$ for NOPA and FNOPAS.

light continuum in NOPA. The remaining beam after BS2 is frequency-doubled in a 1 mm thick second harmonic generation BBO crystal (BBO1), and the output 400 nm beam (60 μJ/pulse) acts as the pump beam of NOPA. To eliminate the anisotropic decay effect of the excited molecules, a half-wave plate WP2 is used to rotate the polarization of excitation beam at a magic angle ($\theta = 54.7°$) with respect to the polarization of the amplified fluorescence (FNOPAS only amplifies the phase-matched polarization of the seeded fluorescence photons). A neutral density filter is used to adjust the excitation intensity. A plano-convex Lens L7 collects and focuses the fluorescence on the BBO crystal in FNOPAS. The reflected beam from BS1 is reflected by a retroreflector on a motorized delay stage, and then it is frequency doubled in a 1 mm thick BBO crystal (BBO3) as the pump beam for FNOPAS. A plano-convex lens L10 ($f = 300$ mm) focuses the pump beam with the focal point located 20 mm behind the BBO crystal in FNOPAS. To test this apparatus, rhodamine 6G ethanol solution was used as the fluorescent sample. During the measurement, the sample solution was continuously stirred in the sample cell having an optical pathlength of 1 mm. Spot sizes of the pump beam and collected fluorescence beam on the FNOPAS crystal are about 600 μm and 400 μm, respectively. The temporal resolution of this FNOPAS was determined as 100 fs by replacing fluorescence seeding light by a small portion of 510 nm light from NOPA.

B. 32-Channel digital lock-in amplifier assisted spectrometer

The amplified fluorescence was focused on the entrance of a 180 mm focal-length spectrograph using either a 300 grooves/mm or a 600 grooves/mm grating by an achromatic lens. The dispersed fluorescence was imaged on the exit plane of the spectrograph where a linear array of quartz fiber bundle consisting of 32 multi-mode optical fibers (core diameter: 400 μm; clad diameter: 500 μm; NA = 0.37) was installed. The 180-mm spectrograph was calibrated with a commercial CCD spectrometer. Consequently, the spectral resolution of the fiber coupled spectrometer was determined as 8.2 nm for the 300 grooves/mm grating and 3.8 nm for the 600 grooves/mm grating. As is shown in Fig. 1, the ends of 32 optical fibers are coupled to 32 standalone Si photodiodes which convert the light intensities of different wavelength to current signals. The current signals are then converted to voltage signals by transimpedance amplifiers with a gain of 4.7×10^7 V/A. The amplified voltage signals are sent to a home-built 32-channel synchronous digital lock-in amplifier, the detail of its design has been described elsewhere.[35] Briefly, the digital lock-in amplifier consists of a field programmable gate array (FPGA) to synchronously communicate with and control ofeight 4-channel synchronous digital lock-in modules.[33] The reference frequency is locked at the optical chopper in the fluorescence excitation beam with a chopping frequency far different from 1 kHz, e.g., 193 Hz as a typical reference frequency. The reference signal is sent to a phase locked loop which provides synchronous clock signals for the digital lock-in modules. The final demodulated signals from FPGA are transferred to a computer via communication interface for further data treatment. Considering the intense parametric superfluorescence background noise which is pumped by the 1 kHz pulsed laser, 32 notch filters with a central cutoff frequency of 1 kHz are designed and connected in the front of each circuit to filter the 1 kHz interference signals associated with the pump laser to improve the signal to noise ratio and dynamic range of our measurement. Comparing with photodiode array, standalone optical fiber coupled photodiodes can eliminate cross talk signal between the neighboring detecting elements. The spectral response of this multi-channel lock-in amplifier assisted spectrometer was calibrated with a commercial spectrometer (HR4000CG-UV-NIR, Ocean Optics). Explicitly, we acquired the steady-state fluorescence spectra of R6G with our 32-channel lock-in amplifier assisted spectrometer and the commercial spectrometer, respectively. The ratio between the two acquired

This article is copyrighted as indicated in the article. Reuse of AIP content is subject to the terms at: http://scitationnew.aip.org/termsconditions. Downloaded to IP: 159.226.35.239 On: Wed, 30 Dec 2015 07:54:51

spectra is taken as the spectral calibration curve for the 32-channel lock-in amplifier assisted spectrometer.

III. RESULTS AND DISCUSSION

To demonstrate the feasibility of this multi-channel lock-in amplifier assisted spectrometer for time-resolved FNOPAS, we measured the transient fluorescence spectra of rhodamine 6G dye in ethanol of varied concentrations. Fig. 2(a) shows a typical amplified fluorescence image as a bright spot on a superfluorescence ring background, where the concentration of rhodamine 6G is 10^{-3}M and the corresponding time-resolved fluorescence spectra and the fluorescence kinetics are displayed in Figs. 3(a) and 3(b), respectively. At this concentration, the fluorescence peak wavelength shows an obvious redshift starting at 30 ps after the excitation, i.e., from 580 nm to 592 nm till 1100 ps, while the fluorescence decay process can be fitted with a monoexponential decay process (τ = 180 ps). With the multi-channel lock-in amplifier assisted fiber-array spectrometer, it took only several minutes to acquire the above time-resolved spectra. As reported previously, under this condition, the time-resolved spectra can also be collected with a CCD assisted spectrometer by the use of background subtraction of an averaged superfluorescence spectrum, since the intensity of the amplified fluorescence is more intense than that of the superfluorescence. However, when the concentration of the dye was reduced to the order of 10^{-4}M, the amplified fluorescence spot cannot be distinguished from the superfluorescence ring as shown in Fig. 2(b), and the method of direct background subtraction fails, indicating that the CCD assisted spectrometer could no longer be used to acquire the time-resolved fluorescence spectra at a concentration lower than 10^{-4}M. In contrast to our previous work, we reduced the lowest concentration from ~10^{-4}M to 10^{-5}M in this work, and the corresponding time-resolved fluorescence spectra and the fluorescence decay kinetics are displayed in Figs. 4(a) and 4(b), respectively. In contrast to those at high concentration, almost no redshift in the spectra can be observed after 2 ps at such a low concentration, and the decay kinetics can be well fitted by a monoexponential

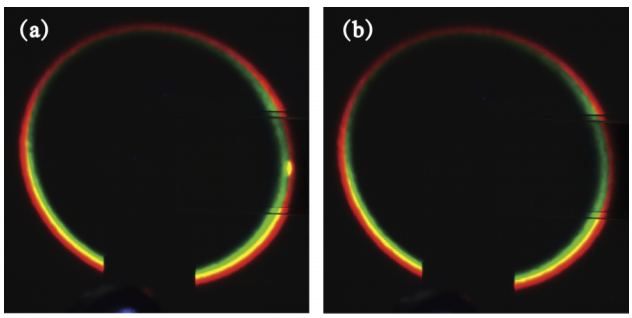

FIG. 2. Far-field image of superfluorescence ring together with the amplified transient fluorescence (bright spot on the right of the superfluorescence ring) of 10^{-3}M (a) and 10^{-4}M (b) rhodamine 6G in ethanol. A rectangular, continuously variable metallic neutral density filter was placed to ensure that both the amplified transient fluorescence and superfluorescence were in the dynamic detection range of the camera. The bright spot arising from 400 nm pump beam at the center of the ring was blocked by a continuously tunable iris.

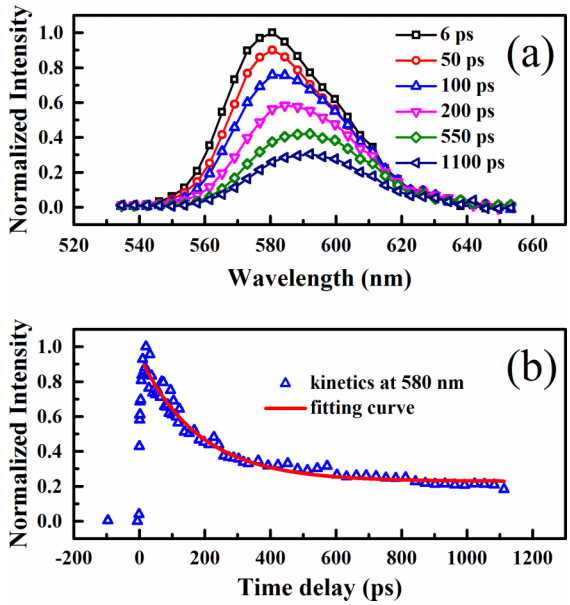

FIG. 3. (a) Transient fluorescence spectra of 10^{-3}M rhodamine 6G in ethanol at different time delays. The solid line is used to guide for view. (b) Decay kinetics at 580 nm (open triangles) and its monoexponential decay fitting curve (solid line), τ = 180 ps.

decay with a time constant of 3.3 ns much longer than that at high concentration, which basically matches a reported lifetime of 3.85 ns measured at a concentration less than 1.5×10^{-6}M.[36] All the time-resolved spectra presented have been corrected for the gain of the BBO crystal according to the reported spectral correction method.[20] Meanwhile, the time-resolved fluorescence spectra were subjected for chirp correction caused by the solvent and optical elements,

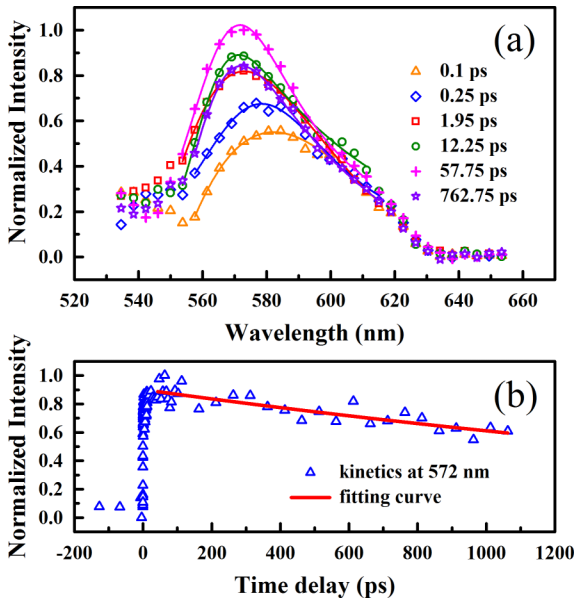

FIG. 4. (a) Transient fluorescence spectra of 10^{-5}M rhodamine 6G in ethanol at different time delays. The solid line is the GaussMod fitted curve for determination of the peak wavelength. (b) Kinetic trace at 572 nm (open triangles) and its monoexponential decay fitting curve (solid line), τ = 3.3 ns. The non-zero background around 540 nm comes from the inference of excitation pulse of 510 nm with a broad bandwidth.

This article is copyrighted as indicated in the article. Reuse of AIP content is subject to the terms at: http://scitationnew.aip.org/termsconditions. Downloaded to IP: 159.226.35.239 On: Wed, 30 Dec 2015 07:54:51

which affects the time zero for different wavelengths. To correct the time zero of time-resolved fluorescence spectra at different wavelength, we employed the white light from the super-continuum generation as the reference. Explicitly, we acquired time zero for the amplified super-continuum white light to quantitatively derive the chirp from the solvent and optical elements at two different conditions, i.e., with and without the solvent in the sample cell, output window of the cell, lens collecting the fluorescence and longpass filter in front of FNOPAS BBO. The resulting difference of time zero between the two measurements is used as chirp from solvent and optical elements for the correction of time-zero position. All the spectra were acquired at room temperature.

Comparing Figs. 3(a) and 4(a), a remarkable difference is that the time-resolved fluorescence spectra of rhodamine 6G solution exhibit a time-dependent redshift in their peak wavelength at the high concentration (10^{-3}M), while such a spectral shift does not appear in those of low concentration (10^{-5}M, also see Fig. 6 for clearer vision). Redshift in the peak fluorescence wavelength of rhodamine 6G in glycerol solution (5×10^{-5}M) has been observed in picosecond time-resolved fluorescence spectra by Kerr gating method as early as in 1974, and this phenomenon has been interpreted in terms of inhomogeneous spectral broadening accompanied by a Stokes shift due to the interaction among the dye and the surrounding solvent molecules.[37] Our results at the low concentration (10^{-5}M) do not support such an interpretation since no spectral shift can be observed after 2 ps. As the redshift in the spectra is concentration dependent, and the fluorescence obviously shows the concentration quenching effect as shown in Fig. 3(b), the fact strongly indicates the formation of the excimer, i.e., an excited dye molecule (A^*) associates with a ground-state molecule (A) to form the excimer ($[A–A]^*$) through effective diffusion and collision at high concentration.[38,39] Accordingly the following reaction schemes can be proposed:

$$A^* \xrightarrow{k_1} A, \tag{1}$$

$$A^* + A \underset{k_3}{\overset{k_2}{\rightleftharpoons}} [A\text{-}A]^*, \tag{2}$$

$$[A\text{-}A]^* \xrightarrow{k_4} [A\text{-}A]. \tag{3}$$

And the corresponding rate equations can be written as

$$\frac{dA^*}{dt} = -(k_1 + k_2 A)A^* + k_3[A\text{-}A]^*, \tag{4}$$

$$\frac{d[A\text{-}A]^*}{dt} = k_2 A A^* - (k_3 + k_4)[A\text{-}A]^*. \tag{5}$$

Therefore, the dye solution should contain two kinds of emissive species, i.e., the excited-state monomer and the excimer. Thus, the experimentally acquired time-resolved fluorescence spectra should also consist of two types of spectra correspondingly.

To resolve the individual spectral components from the as-acquired spectra, we employed the method of singular value decomposition (SVD) to resolve the species-associated emission spectra and the corresponding kinetics according to the reported procedures.[39–41] Fig. 5(a) presents the

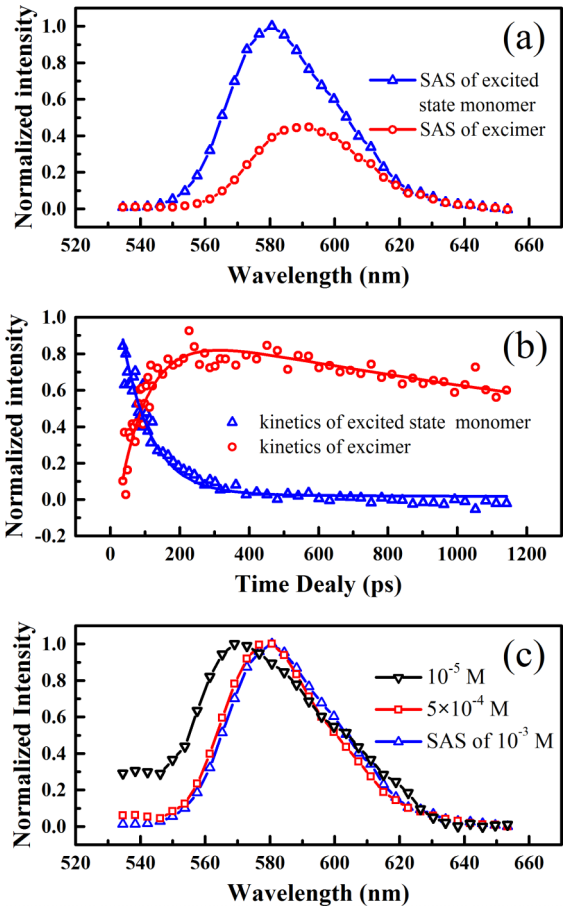

FIG. 5. (a) SVD-resolved two species associated spectra (SAS) assigned to the excited-state monomer (open triangles) and the excimer (open circles), respectively (the solid line is used to guide for view). (b) SVD-resolved species-associated kinetics for the excited-state monomer (open triangles) and the excimer (open circles). (c) Comparison of the SVD-resolved monomer fluorescence spectrum (open triangles) with that obtained directly by FNOPAS at low concentrations of 10^{-5}M and 5×10^{-4}M rhodamine 6G solution (the solid line is used to guide for view).

SVD resolved species associated spectra (SAS) of 10^{-3}M rhodamine 6G in ethanol and the corresponding population evolution kinetics are shown in Figs. 5(b) and 5(c) compares the SAS of the fast decay component with the experimentally collected one at two different lower concentrations (10^{-5}M and 5×10^{-4}M) after 2 ps. For these two concentrations no observable spectral shift can be observed after 2 ps (see Fig. 7(a)). Obviously the SAS of the fast decay component of 10^{-3}M solution is basically same as the fluorescence spectrum of 5×10^{-4}M solution. We also noted that the time-resolved fluorescence spectra of 10^{-5}M and 5×10^{-4}M solutions having 10 nm difference in their peak wavelengths. A possible cause will be given later in this section (see discussion about Fig. 7). The fluorescence spectrum for 10^{-5}M solution is believed as that of the excited-state monomer at such a low concentration, since it has been reported that the ground-state dimer would be formed only when the concentration exceeds 10^{-2}M.[42] If we neglect the spectral difference between these two lower concentrations, i.e., also assume that rhodamine 6G molecules still exist as monomer at the concentration of 5×10^{-4}M, we can assign the SAS of the fast decay component to that of the excited-state monomer, and the

This article is copyrighted as indicated in the article. Reuse of AIP content is subject to the terms at: http://scitationnew.aip.org/termsconditions. Downloaded to IP: 159.226.35.239 On: Wed, 30 Dec 2015 07:54:51

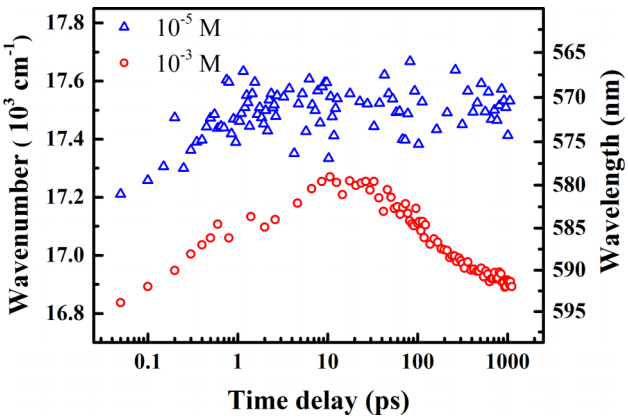

FIG. 6. Time-dependent peak wavelength of the fluorescence spectra acquired for 10^{-5}M and 10^{-3}M rhodamine 6G ethanol solutions.

remaining SAS of slow decay component would be from the excimer accordingly. To fit the SVD-resolved population evolution kinetics globally, we solved the rate Equations (4) and (5) numerically by using Runge–Kutta method with an initial condition of $A^*_{t=0} = 1$ and $[A\text{-}A]^*_{t=0} = 0$. We used Levenberg–Marquardt algorithm to search the values for k_1, k_2, k_3, and k_4 which best fit the population evolution kinetics. The fitted curves are shown in Fig. 5(b) as the solid curves, where $k_1 = 1/1910$ (ps)$^{-1}$, $k_2 = 1.1 \times 10^{13}$ s^{-1}M^{-1}, $k_3 = 1/3240$ ps^{-1}, and $k_4 = 1/2285$ ps^{-1}. From the global fitting, we got the radiative decay lifetime for the fast decay component of 1.9 ns ($1/k_1$) which can be compared to that of

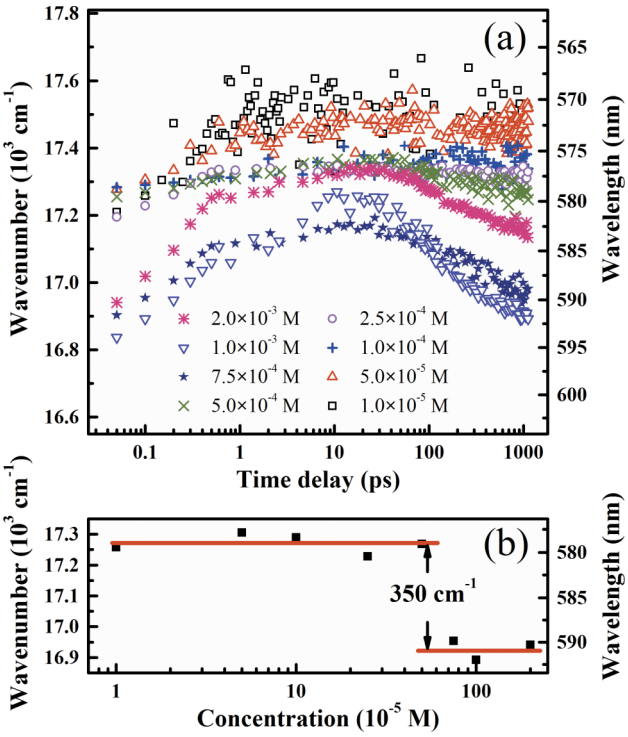

FIG. 7. (a) Time-dependent peak wavelength of the fluorescence spectra acquired for a series of rhodamine 6G ethanol solutions of varied concentration. (b) Plot of the initial peak wavelength at t = 0.1 ps against the concentration. The horizontal lines denote the positions of the two averaged peak wavelengths, respectively.

5×10^{-4}M solution (1.5 ns) directly fitted by monoexponential decay; and a lifetime for the excimer of 2.3 ns ($1/k_4$) is also basically consistent with the reported lifetime for the excited dimer in methanol of 4.6 ns considering our limited optical delay line of 1.1 ns.[42]

To further confirm the above mechanism, as well as to illustrate the solvation process, we acquired time-resolved fluorescence spectra for a series of samples with a varied concentration at a better temporal and spectral resolution as suggested by the reviewers. As we have shown that the spectral resolution of the apparatus is 3.8 nm, while in the post-data analysis, we used GaussMod function embedded in Origin software to fit the acquired spectra (see Fig. 4(a)), and the peak position of the time-resolved fluorescence spectra can be found with an improved spectral resolution. Fig. 6 plots the obtained fluorescence peak wavelength against the time for two different concentrations, i.e., 10^{-5}M and 10^{-3}M.

As shown in Fig. 6, at a low concentration (open triangle), about 10 nm spectral shift can be observed within the first 10 ps, then there is no spectral shift in the later time. We then inspected the time-resolved fluorescence peak shift in a much higher concentration of 10^{-3}M shown in Fig. 6 (open circle). In this case, the spectral blueshift in the first stage is still there within the first 10 ps, the time-dependent spectral shift can be fitted by a monoexponential process with a time constant of 2.4 ps. Referring to the solvation process of Coumarin 153 probed by the dynamic Stokes shift in the peak fluorescence, which has a time constant ranging from about 2 ps to 10 ps with a relative large Stokes shift (redshift about 2000 cm^{-1} measured in a concentration of 5×10^{-5}M);[43] thus, we attribute the first stage to the solvation process of rhodamine 6G in ethanol. However, the spectral shift observed in our experiment was blue shift. The spectral shift can be observed in a steady-state and a nonequilibrium state. For steady-state spectra, solvation can cause either a blue or a red shift in the absorption or emission spectra depending on the relative magnitude of the dipole-moment of the ground and the excited state, i.e., μ_g and μ_e. For the case of the blue shift, μ_g should be larger than μ_e ($\mu_g > \mu_e$); and it is reversed for the case of red shift.[44,45] For nonequilibrium state, blue shift has been scarcely observed. Levy *et al.* have conducted molecular dynamical simulation of time-resolved fluorescence and nonequilibrium solvation of formaldehyde in water; they found that a dynamical blue shift occurs within the first ps of solvation, which also requires $\mu_g > \mu_e$. A physical account for this is that the excited state is more favorably solvated by the solvent structure organized around the ground state indicating a larger stabilization energy at the initial time of the excitation pulse, because the excited-state species having a smaller dipole moment will not be able to keep the solvent molecules as tight as the ground-state species; the solvation (stabilization) energy decreases with time as the solvent structure relaxes, which would lead to a dynamical blue shift in the time-resolved fluorescence spectra.[46] In the current work, we have observed a dynamical blue shift in the time-resolved fluorescence spectra. For rhodamine 6G, it has been reported that $\mu_g = 16.1$ and $\mu_e = 10.5$ (Debye), respectively;[47] therefore, the observed dynamical blue shift in the first ps can be plausibly ascribed to the solvation process.

This article is copyrighted as indicated in the article. Reuse of AIP content is subject to the terms at: http://scitationnew.aip.org/termsconditions. Downloaded to IP: 159.226.35.239 On: Wed, 30 Dec 2015 07:54:51

Interestingly, a remarkable difference in the time-dependent peak wavelength appears in the second stage, i.e., starting at 30 ps, the fluorescence peak wavelength exhibits a monotonical redshift from 580 nm to 592 nm, which is clearly missing in that of the low concentration. The fact obviously supports the excimer formation mechanism we proposed based on the SVD analysis.

Fig. 7(a) gives more time-dependent fluorescence peak wavelength in a series of sample of varied concentration. Obviously, all the initial peak wavelengths (0.1 ps after time zero) can be classified into two groups of low and high concentrations (Fig. 7(b)), i.e., 579 nm (17 271 cm^{-1}) (averaged value) for low concentration and 591 nm (16 921 cm^{-1}) (averaged value) for high concentration. It has been observed that the rhodamine 6G forms unstable ground-state dimer with a binding energy less than 1 kT at a concentration larger than 10^{-2}M in methanol;[42] therefore, our result in Fig. 7(b) strongly suggests that ground-state loosely bound pairs might be formed at a concentration about 5×10^{-4}M with a calculated binding energy about 350 cm^{-1} (1.7 kT) in ethanol. It is noted that the theoretical calculation of the ground-state dimer shows that the J-aggregate form (head-to-tail) of rhodamine 6G would lead to a redshift in the absorption spectrum with respect to that of the monomer, and the predicted energy difference between the absorption maxima is 0.098 eV (792 cm^{-1}),[48] which indicates that the ground-state loosely bound pair would be less stable than the ground-state dimer.

We then conducted SVD analysis on the measured time-resolved fluorescence spectra of rhodamine 6G solutions with a series of different concentrations. Only some of the spectra at a concentration of 10^{-4}, 2.5×10^{-4}, 5×10^{-4}, 7.5×10^{-4}, 10^{-3}, and 2×10^{-3}M can be analyzed successfully by the SVD method. The corresponding pseudo first-order rate constant (k_2A) can be obtained. A plot of these rate constants against the concentration of the dye is shown in Fig. 8, in which the second order rate constant (k_2) for the formation of the excimer can be obtained, which has a value of 1.07×10^{13} $s^{-1}M^{-1}$. This value is apparently larger than the generally observed diffusion-limited bimolecular rate constant at room temperature in an order of 10^{10} $s^{-1}M^{-1}$.[49] Lawandy *et al.* have reported the phenomenon of laser inhibited diffusion in rhodamine ethanol solutions, they found that the diffusion constant of the singlet-excited state rhodamine 6G is only 1/18 of that of the ground state.[50] Therefore, the observed larger second-order rate constant for the formation of the excimer cannot be interpreted by the diffusion rate constant of the singlet-excited state molecule, instead the much larger rate constant also points to the formation of the ground-state loosely bound pair. We noted that the pseudo first-order rate constant for 2×10^{-3}M solution is almost same as that of 10^{-3}M, which indicates that the ground-state loosely bound pair would begin to form ground-state dimer at a concentrated solution higher than 1×10^{-3}M, for this would lead to a concentration independent pseudo first-order rate constant.

Based on the above analysis, it is quite clear that the observed redshift in the fluorescence peak wavelength with respect to that of the excited monomer after 30 ps for the concentrated rhodamine 6G solution is caused by the formation of excimer from the ground-state loosely bound pair. The energy diagram for the ground-state loosely bound pair and excimer is shown in Fig. 9, where the coupling matrix element |V| for the excimer $[A–A]^*$ can be estimated from the difference in the emission peaks of excimer and the excited state of the ground-state loosely bound pair $[A^*–A]$, i.e., |V| = 0.036 eV or 292 cm^{-1}. There the formation energy of the excimer (energy difference between the excimer and the monomer) should be the sum of the binding energy of the ground-state loosely bound pair and the above coupling matrix element, i.e., 642 cm^{-1} (0.08 eV, or 3.1 kT). Interestingly, Lawandy *et al.* reported an energy difference between the excited state and the ground-state rhodamine 6G in ethanol of 3 kT in a concentration range of 10^{-4} to 10^{-3}M at room temperature;[50] thus, their value is quite consistent to the energy difference between the excimer and the monomer in the current case.

To test the background noise rejection capability, we collected the superfluorescence intensities at a selected area on the superfluorescence ring under rejected and un-rejected mode, respectively. The intensity of the rejected superfluorescence was simply collected by blocking the seeding fluorescence with chopper modulation on the fluorescence excitation beam, while the intensity of the un-rejected superfluorescence was measured by moving the chopper from the excitation beam to the pump beam with the seeding fluorescence being blocked. The calculated ratio

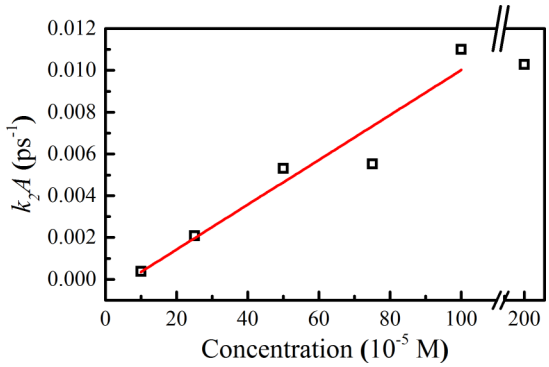

FIG. 8. Pseudo first-order rate constant against the concentration. The solid line is the linear fitted curve for all the data points except for the last one.

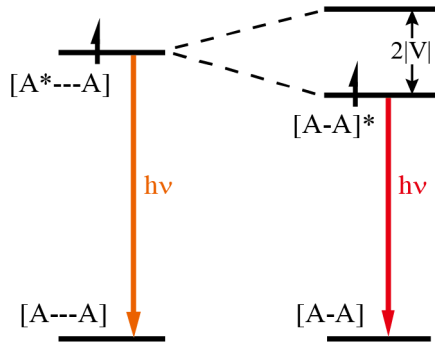

FIG. 9. The energy diagram for the relation between the excimer and the ground-state loosely bound pair, |V| is the coupling matrix element for the excimer.

This article is copyrighted as indicated in the article. Reuse of AIP content is subject to the terms at: http://scitationnew.aip.org/termsconditions. Downloaded to IP: 159.226.35.239 On: Wed, 30 Dec 2015 07:54:51

between the two intensities of rejected and un-rejected superfluorescence ranges between 1/300 and 1/100.

Finally, we used 10^{-5}M rhodamine 6G in ethanol excited at 510 nm with an excitation intensity of 70 nJ/pulse to determine the detection limit of our system. The gain factor of the FNOPAS was determined to be about 4.2×10^3 at a pump intensity of 60 μJ/pulse with the method reported previously.[19] The lowest detectable amplified fluorescence signal at 610 nm with a time delay of 1100 ps was measured, which is equivalent to about 18 fJ/pulse, corresponding to 5.3×10^4 photons/pulse. This corresponds to a fluorescence detection limit of about 13 seeding fluorescence photons/pulse.

IV. CONCLUSION

We have developed a femtosecond time-resolved fluorescence spectroscopy setup which realizes background free detection of broadband fluorescence spectra with a home-made 32-channel lock-in amplifier. The superfluorescence background signal can be significantly reduced down to 1/300–1/100. Temporal synchronization of 32 channels avoids the wavelength scanning in single-wavelength detection mode. This has an advantage of reducing the measuring time and eliminating the time jitter at different wavelength for construction a reliable time-resolved fluorescence spectrum. Transient fluorescence spectra of 10^{-5}M rhodamine 6G dye in ethanol have been successfully detected by the current apparatus, which could not be realized with CCD assisted spectrometer. Concentration dependent spectral shift in time-resolved fluorescence spectra of this dye have also been observed, and we proposed an excimer formation model to account for the observed concentration-dependent spectral shift. The improvement of the detection system would definitely make FNOPAS a more powerful tool in ultrafast time-resolved fluorescence spectroscopic studies.

ACKNOWLEDGMENTS

This work is supported by National Key Foundation for Developing Scientific Instrument (No. 2013YQ030595) and the Natural Science Foundation of China (Grant No. 21227003).

[1]T. Damen and J. Shah, Appl. Phys. Lett. **52**, 1291 (1988).
[2]H. Szmacinski and J. R. Lakowicz, Sens. Actuators, B **29**, 16 (1995).
[3]B. Gobets, J. T. Kennis, J. A. Ihalainen, M. Brazzoli, R. Croce, I. H. van Stokkum, R. Bassi, J. P. Dekker, H. van Amerongen, and G. R. Fleming, J. Phys. Chem. B **105**, 10132 (2001).
[4]R. V. Krishnan, E. Biener, J.-H. Zhang, R. Heckel, and B. Herman, Appl. Phys. Lett. **83**, 4658 (2003).
[5]I. v. Stokkum, B. Gobets, T. Gensch, F. v. Mourik, K. Hellingwerf, R. v. Grondelle, and J. Kennis, Photochem. Photobiol. **82**, 380 (2006).
[6]S. Arzhantsev and M. Maroncelli, Appl. Spectrosc. **59**, 206 (2005).
[7]H. Lemmetyinen, N. V. Tkachenko, B. Valeur, J. Hotta, M. Ameloot, N. P. Ernsting, T. Gustavsson, and N. Boens, Pure Appl. Chem. **86**, 1969 (2014).
[8]B. Schmidt, S. Laimgruber, W. Zinth, and P. Gilch, Appl. Phys. B **76**, 809 (2003).
[9]I. Eom and T. Joo, J. Chem. Phys. **131**, 244507 (2009).
[10]J. Takeda, K. Nakajima, S. Kurita, S. Tomimoto, S. Saito, and T. Suemoto, Phys. Rev. B **62**, 10083 (2000).
[11]C. Ma, W. M. Kwok, W. S. Chan, P. Zuo, J. T. W. Kan, P. H. Toy, and D. L. Phillips, J. Am. Chem. Soc. **127**, 1463 (2005).
[12]H. Mahr and M. D. Hirsch, Opt. Commun. **13**, 96 (1975).
[13]L. Zhao, J. L. P. Lustres, V. Farztdinov, and N. P. Ernsting, Phys. Chem. Chem. Phys. **7**, 1716 (2005).
[14]M. Branderhorst, P. Wasylczyk, and I. Walmsley, Appl. Phys. Lett. **88**, 061109 (2006).
[15]X.-X. Zhang, C. Wurth, L. Zhao, U. Resch-Genger, N. P. Ernsting, and M. Sajadi, Rev. Sci. Instrum. **82**, 063108 (2011).
[16]M. Sajadi, M. Quick, and N. P. Ernsting, Appl. Phys. Lett. **103**, 173514 (2013).
[17]P. Fita, Y. Stepanenko, and C. Radzewicz, Appl. Phys. Lett. **86**, 021909 (2005).
[18]X.-H. Chen, X.-F. Han, Y.-X. Weng, and J.-Y. Zhang, Appl. Phys. Lett. **89**, 061127 (2006).
[19]X.-F. Han, X.-H. Chen, Y.-X. Weng, and J.-Y. Zhang, J. Opt. Soc. Am. B **24**, 1633 (2007).
[20]H. Chen, Y. Weng, and J. Zhang, J. Opt. Soc. Am. B **26**, 1627 (2009).
[21]W. Dang, P. Mao, and Y. Weng, Rev. Sci. Instrum. **84**, 073105 (2013).
[22]Y. Weng, X. Han, and J. Zhang, J. Opt. Soc. Am. B **25**, 1627 (2008).
[23]X.-F. Han, Y.-X. Weng, R. Wang, X.-H. Chen, K.-H. Luo, L.-A. Wu, and J. Zhao, Appl. Phys. Lett. **92**, 151109 (2008).
[24]A. Shirakawa and T. Kobayashi, IEICE Trans. Electron. **E81-C**, 246 (1998).
[25]X.-F. Han, Y.-X. Weng, A. Pan, B. Zou, and J.-Y. Zhang, Appl. Phys. Lett. **92**, 032102 (2008).
[26]H. Chen, W. Dang, J. Xie, J. Zhao, and Y. Weng, Photosynth. Res. **111**, 81 (2012).
[27]H.-L. Chen, Y.-X. Weng, and X.-Y. Li, Chin. J. Chem. Phys. **24**, 253 (2011).
[28]Q. Liao, Z. Xu, X. Zhong, W. Dang, Q. Shi, C. Zhang, Y. Weng, Z. Li, and H. Fu, J. Mater. Chem. C **2**, 2773 (2014).
[29]D. A. Kleinman, Phys. Rev. **174**, 1027 (1968).
[30]T. G. Giallorenzi and C. L. Tang, Phys. Rev. **166**, 225 (1968).
[31]P. Ditrapani, A. Andreoni, G. P. Banfi, C. Solcia, R. Danielius, A. Piskarskas, P. Foggi, M. Monguzzi, and C. Sozzi, Phys. Rev. A **51**, 3164 (1995).
[32]C. Homann and E. Riedle, Laser Photonics Rev. **7**, 580 (2013).
[33]A. Restelli, R. Abbiati, and A. Geraci, Rev. Sci. Instrum. **76**, 093112 (2005).
[34]K. Seto, Y. Okuda, E. Tokunaga, and T. Kobayashi, Rev. Sci. Instrum. **84**, 083705 (2013).
[35]K. Chen, X.-C. Liu, X.-W. Luo, X.-L. Zhou, W. Peng, and Q.-X. Yu, J. Optoelectron. **26**, 116 (2015).
[36]F. López Arbeloa, T. López Arbeloa, M. Tapia Estevez, and I. López Arbeloa, J. Phys. Chem. **95**, 2203 (1991).
[37]M. M. Malley and G. Mourou, Opt. Commun. **10**, 323 (1974).
[38]S. A. Jenekhe and J. A. Osaheni, Science **265**, 765 (1994).
[39]Y. Wang, H. Chen, H. Wu, X. Li, and Y. Weng, J. Am. Chem. Soc. **131**, 30 (2009).
[40]L. Zhang, J. Yang, L. Wang, G.-Z. Yang, and Y.-X. Weng, J. Phys. Chem. B **107**, 13688 (2003).
[41]S. Yamaguchi and H. Hamaguchi, J. Chem. Phys. **109**, 1397 (1998).
[42]A. Penzkofer and W. Leupacher, J. Lumin. **37**, 61 (1987).
[43]M. L. Horng, J. A. Gardecki, A. Papazyan, and M. Maroncelli, J. Phys. Chem. **99**, 17311 (1995).
[44]C. Reichardt, Chem. Rev. **94**, 2319 (1994).
[45]A. Yu, C. A. Tolbert, D. A. Farrow, and D. M. Jonas, J. Phys. Chem. A **106**, 9407 (2002).
[46]R. M. Levy, D. B. Kitchen, J. T. Blair, and K. Krogh-Jespersen, J. Phys. Chem. **94**, 4470 (1990).
[47]S. Kinoshita and N. Nishi, J. Chem. Phys. **89**, 6612 (1988).
[48]V. I. Gavrilenko and M. A. Noginov, J. Chem. Phys. **124**, 044301 (2006).
[49]Y.-X. Weng, K.-C. Chan, B.-C. Tzeng, and C.-M. Che, J. Chem. Phys. **109**, 5948 (1998).
[50]N. M. Lawandy, P. L. Fuhr, and D. Robinson, Phys. Lett. A **84**, 137 (1981).

This article is copyrighted as indicated in the article. Reuse of AIP content is subject to the terms at: http://scitationnew.aip.org/termsconditions. Downloaded to IP: 159.226.35.239 On: Wed, 30 Dec 2015 07:54:51